OPTIMIZATION AND MODELING OF THE ACCELERATOR FOR THE FERMI @ ELETTRA FEL

S. Di Mitri*, M. Cornacchia, P. Craievich, Sincrotrone Trieste S.C.p.A., Trieste, Italy
P. Emma, Z. Huang, J. Wu, SLAC, Menlo Park, California
D. Wang, MIT, 77 Massachusetts Avenue Cambridge, Massachusetts
A. Zholents, LBNL, Berkeley, California

Abstract

Design studies are in progress to use the existing FERMI@Elettra linear accelerator for a seeded harmonic cascade free-electron laser (FEL) facility [1]. This accelerator will be upgraded to 1.2 GeV and equipped with a low-emittance RF photocathode gun, laser heater, two bunch compressors, and a beam delivery system. We present an optimization study of all the components downstream of the gun, aimed at achieving the high peak current, low energy spread and low emittance electron beam necessary for the FEL. Various operational scenarios are discussed. Results of accelerator simulations including effects of space charge, coherent synchrotron radiation and wakefields are reported.

I. INTRODUCTION

Reference [1] contains general description of the FEL facility to be built at Sincrotrone Trieste based on the 1.2 GeV linac. The FEL part of this facility is described in Ref. [2] and the injector part in Ref. [3].

In this paper we address a beam delivery system starting from the end of the injector and ending at the entrance of the FEL. This system includes four linac sub-sections, two bunch compressors, a vertical ramp and a beam switch yard (spreader) between two FELs. Figure 1 shows a schematic of the facility.

The main task for the beam delivery system is beam acceleration and compression while maintaining a low energy spread and emittance. Along this process the beam quality is affected by space charge, wakefields, coherent synchrotron radiation (CSR) and other detrimental effects. We have carried out an optimization study for the locations of the accelerating sections and bunch compressors, for the compression efficiency, for the magnitude of the beam energy chirp at various stages of acceleration, for the electron beam optics in the linac sections, bunch compressors, vertical ramp and spreader, including provisions for beam diagnostics.

The optimization was done for two operational scenarios: the "short bunch option", where the accelerator delivers a beam with ~200 fs bunch length and 800 A peak current, preferable for FEL1 with one cascade, and the "long bunch option", where the accelerator delivers a beam with ~1 ps bunch length with reduced peak current of 400 A, preferable for FEL2 with two cascades. In this paper we report the studies of the short bunch scenario which is at present in a more advanced stage. In Section II the three types of linac sub-sections that will be used for acceleration are presented, together with a discussion of the wakefields they produce. In Section III the beam optics of the entire beam delivery system is presented. In Section IV and V we discuss collective effects and present the results of particle tracking.

II. LINAC

Three types of accelerating sections constitute the Fermi linac. The S0A and S0B sections (yellow colored in Fig.1) are placed just after the gun and are used for the emittance compensation scheme. Seven CERN-type sections (C1-C7, green colored in Fig.1) are used before and after the first chicane. Both S0A and S0B and CERN sections are traveling wave (TW) structure which work in the 2/3π mode and coupled on axis [4, 5]. Seven Elettra-sections (S1-S7, blue coloured in Fig.1) cover the last part of the linac. Each section is a backward traveling wave (BTW) structure composed by 162 nose cone cavities magnetically coupled and operated in the 3/4π mode [6]. Table 1 summarizes the main RF parameters and basic dimensions.

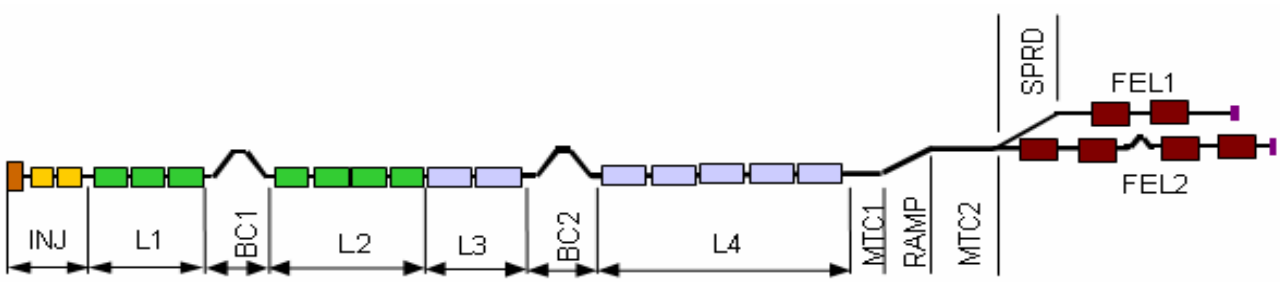

Figure 1: Schematic layout for the Fermi project. The RAMP is in the vertical plane, while the SPRD is in the horizontal.

*simone.dimitri@elettra.trieste.it

Table 1. Main parameters and basic dimensions of the three accelerating sections. (In table a is the iris radius, b is the outer radius, L is the cell length and g is the gap length.)

	S0A, S0B	CERN	BTW
Mode	TW 2/3π	TW 2/3π	BTW 3/4π
f [MHz]	2997.747[M]	-	2997.74[M]
a [mm]	9.73 (av.)	10.75 (av.)	5.0
b [mm]	39[D]	41.75	39[D]
L [mm]	33.33[D]	33.321	37.5[D]
g [mm]	30.43	30.33	-
cells[1]	93	135	162
L_{tot} [mm]	3200	4500	6150
Q	14100[M]	-	11700[M]
R0 [MΩ/m]	67.1[S]	-	-
E [MV/m]	14.1[D]	10.4[D]	19.5[D]
Gain [MV]	45.5[D]	47[D]	120[D]

[1]without input and output cells, [S]electromagnetic simulation
[M]measured, [D]technical design or estimated

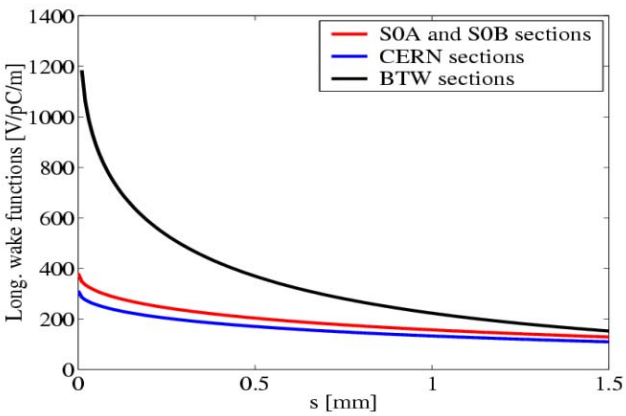

Figure 2: Longitudinal wake functions for the accelerating section used in the FERMI linac.

The wake functions for all three types of accelerating sections have been calculated in [7] using an analytical approximation from [8, 9] for S0A, S0B and CERN sections and a time domain code for BTW sections [10]. Figures 2 and 3 show respectively the longitudinal and transverse wake functions calculated up to the distance of 1.5 mm. Wake functions for the BTW sections are strongest because of their smaller iris radius.

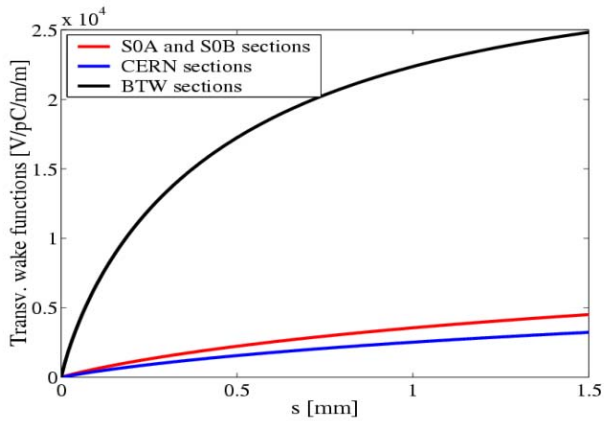

Figure 3: Transverse wake functions for the accelerating sections used in the FERMI linac.

III. OPTICS

A FODO optics is used in the linac with a maximum beta-function less than 40 m to minimize the chromatic effects on the transverse emittance. Optics of two bunch compressors is designed with a minimum of the horizontal beta-function positioned within the last of four bending magnets of magnetic chicanes. This minimizes emittance increase due to the CSR. In a short bunch option, the first bunch compressor BC1 (see, Figure 1) is set to compress a 5 ps (FWHM) electron bunch to approximately 1.4 ps using a time-of-flight parameter R_{56}=6.9 cm and the second bunch compressor BC2 compresses it further to the entire length of 450 fs using R_{56}=2.9 cm.

The electron beam is transported into the undulator hall from the end of the linac tunnel using vertical ramp lattice [11]. Four bending magnets are used there. The first two magnets tilt the beam trajectory up by 12.5° and the last two bending magnets bring it into horizontal plane approximately 4.9 m above the linac tunnel. All bending magnets are separated by *–I* transport matrixes in both planes. This arrangement provides compensation of the emittance induced due to CSR in the first pair of magnets by CSR in the second pair of the magnets. The vertical ramp is made to be isochronous. It allows effective emittance compensation even in a case of a relatively large energy chirp within the electron bunch. Provisions for measurements of a slice energy spread in a high dispersion point using the rf sweep and beam collimation in a high beta points are also included into the ramp lattice [12,13].

The vertical ramp is followed by the FODO diagnostic beamline and a spreader. The spreader sets the FEL1 aside from the FEL2 by approximately 2m (see, Figure 1). The electron bunch can either go into the FEL2 when the first bend magnet in the spreader is switched off or into the FEL1 when this magnet is on. The spreader lattice is similar to the vertical ramp lattice.

IV. COLLECTIVE EFFECTS

Wakefields, CSR, space charge and microbunching instability play a major role in electron beam dynamics.

Wakefields

The longitudinal wakefields in the accelerating sections L1 – L3 had been used in a combination with off-crest acceleration in order to control an energy chirp along the electron bunch before BC1 and BC2. The longitudinal wakefields and off-crest acceleration in L4 had been used to cancel the energy chirp at the end of the linac.

Jitters in the phase and amplitude of the accelerating fields as well as a jitter in the electron bunch charge and emission time affect the machine performance. We studied sensitivity of the peak current, beam energy and electron bunch arrival time at the end of the linac to the various jitters and create a tolerances budget shown in Table 2 [14].

Table 2. Rms tolerance budget for <10% rms peak current jitter or <0.1% rms final energy jitter or <200 fs final timing jitter. The tighter tolerance is in bold and all criteria are satisfied with the tighter tolerance applied. Symbols refer to Fig.1; L0 is S0B (the 2nd accelerating section of the Injector).

Parameters		Unit	$\lvert\Delta E/E_0\rvert$ <0.1%	$\lvert\Delta I/I_0\rvert$ <10%	$\lvert\Delta t_f\rvert$ <200fsec
L0	φ_0	deg	**0.30**	**0.30**	0.90
L1	φ_1	deg	**0.18**	0.19	0.19
L2	φ_2	deg	**0.18**	**0.18**	**0.18**
L3	φ_3	deg	**0.18**	0.30	**0.18**
L4	φ_4	deg	**0.50**	1.00	2.67
L0	$\Delta V_0/V_0$	%	**0.15**	0.30	0.30
L1	$\Delta V_1/V_1$	%	**0.15**	0.18	0.18
L2	$\Delta V_2/V_2$	%	**0.15**	0.40	0.18
L3	$\Delta V_3/V_3$	%	**0.15**	0.35	0.18
L4	$\Delta V_4/V_4$	%	**0.10**	2.70	0.10
Gun	Δt_0	psec	**0.15**	**0.15**	**0.15**
	$\Delta Q/Q$	%	**4.00**	**4.00**	**4.00**

Transverse wake fields cause coherent oscillation of electrons in the bunch with respect to the trajectory of the electrons in the head of the bunch. The amplitude of the oscillation increases towards the tail of the bunch causing an increase of the projected emittance. Simulations show that transverse wakefields of the BTW structures aligned with the rms error 0.2 mm can drive these oscillations up to 0.3 mm in amplitude. Transverse wakefields of the other structures are weaker (see, Figure 3) and less damaging. Fortunately, transverse wakefields can be neutralized using beam based tuning, *i.e,* first, by correcting a trajectory and, second, by applying closed trajectory bumps and letting wakefields of one group of cavities to compensate effect of the wakefields of the other cavities. For example, employing both techniques in simulations we were able to reduce the normalized projected emittance from 10 μm to 3 μm [7].

CSR

CSR in the BC1 and BC2 and bending magnets of the vertical ramp and spreader can increase projected emittance. We control this increase by a properly chosen optics as discussed in Section III. CSR wakefield also causes energy variation along the electron bunch. The effect of this wake field is partially compensated by the accelerating rf fields when off-crest positions for acceleration is used. Nevertheless, simulations show that CSR contributes to a slice energy spread about 50 keV.

Space charge and microbunching instability

Microbunching instability and longitudinal space charge effect had been studied before in various cases, most recently in [15]. The essence of the problem is that density modulations on the beam due to a shot noise or some other external source of modulation are amplified by the longitudinal space charge and beam compression in bunch compression chicanes.

Following [15] we analyse possible implication of those effects to FERMI accelerator using actual lengths of different accelerating sections and actual strengths of the bunch compressors. In result we calculate the gain of the instability as a function of the wavelength of the density modulation in the electron bunch emerging out of the gun and plot it in Figure 4. For this calculation we assumed 3 keV initial uncorrelated energy spread.

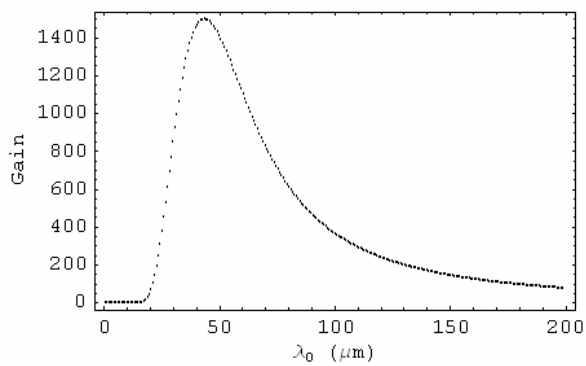

Figure 4: Spectral gain function of the microbunching instability.

Using the function plotted in Figure 4 and assuming a uniform spectral noise power in the beam after the gun defined by the shot noise, we calculate that the microbunching instability will increase slice energy spread at the end of the linac up to 220 keV.

"Laser heater" was proposed in [16] in order to damp microbunching instability. It produces a controlled increase of the uncorrelated energy spread and essentially increases the Landau damping. We calculated slice energy spread at the end of the linac for different setting of the laser heater and plotted it in Figure 5. The minimum slice energy spread there is approximately 80 keV. This must be added to the slice energy spread due to CSR.

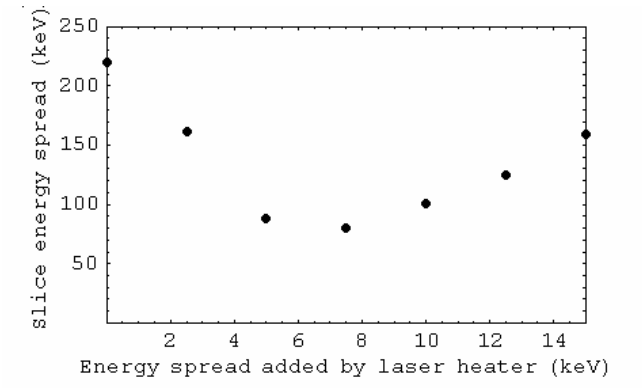

Figure 5: Slice energy spread at the end of the linac as a function of the magnitude of the artificially added energy spread using laser heater.

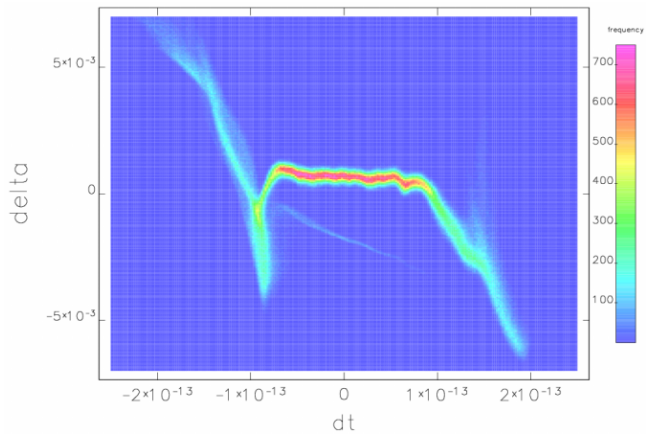

Figure 6: Longitudinal phase space (temporal position versus relative energy spread) at the end of the spreader.

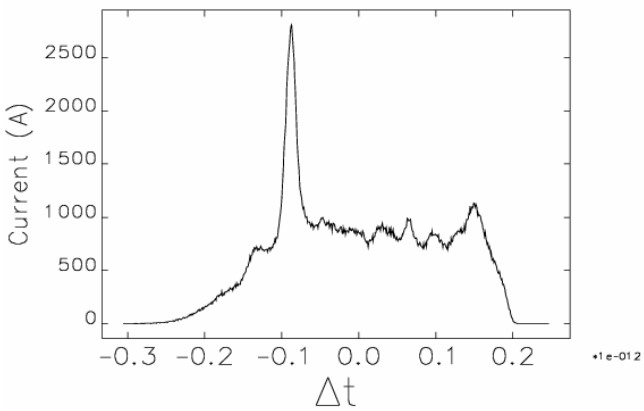

Figure 7: Electron beam peak current at the end of the spreader. Elegant tracking with 1 million macroparticles.

V. PERFORMANCE

We performed particle tracking for a short bunch option using Elegant [17] beginning from S0B accelerating section. Input particle distribution was taken from the output of the electron gun simulations [3]. In the course of this work we found that numerical noise coming from the binning and granularity of macroparticles dominates the machine performance even with 10^6 macroparticles, *i.e.* it provided a stronger than necessary seed for microbunching instability. By temporally excluding longitudinal space charge effects from modeling we mostly eliminated this problem. Plans are considered to solve this problem by calculating the evolution of the distribution function.

Figure 6 shows the longitudinal phase space at the end of the spreader. In this tracking laser heater was set to add 8 keV to the uncorrelated energy spread. Figure 7 shows a histogram of the peak current for the same beam. Several global electron beam parameters are given in Table 3.

Table 3. Electron beam parameters for a short bunch option.

Bunch charge	330	pC
Beam energy	1.2	GeV
Peak current (beam core)	0.8	kA
Bunch duration (full width, beam core)	200	fs
Slice energy spread (rms, beam core)	150	keV
Slice emittance (rms, beam core)	1.2	μm
Laser heater (energy spread rms)	8	keV
Compression factor in BC1 (nominal)	3.5	-
Compression factor in BC2 (nominal)	3.0	-

REFERENCES

[1] C. Bocchetta *et al.*, this conference.
[2] G. De Ninno, *et al.*, this conference.
[3] G. Penco *et al.*, this conference.
[4] G. D'Auria, ST/M-TN-90/15, August 1990.
[5] G. D'Auria, private communication.
[6] G. D'Auria, C. Rossi, ST/M-TN-91/15, July 1991.
[7] S. Di Mitri, *et al.*, ST/F-TN-05/01, Trieste, Italy
[8] K. Bane *et al.*, SLAC-PUB-7862, (1998).
[9] K. Bane, SLAC-PUB-9663, (2003).
[10] P. Craievich, T. Weiland and I. Zagorodnov, 8th ICAP, June 2004, St. Petersburg, Russia.
[11] A. Zholents, CBP Tech Note-334, February 2005.
[12] A. Zholents, CBP Tech Note-348, August 2005.
[13] M. Ferianis *et al.*, this conference.
[14] G. D'Auria *et al.*, this conference
[15] Z. Huang *et al.*, Phys. Rev. ST-AB, **7**, 074401 (2004).
[16] E. Saldin *et al.*, NIM A **528,** 355(2004).
[17] M. Borland, APS LS-207, (2000).